AGU PUBLICATIONS

Tectonics

RESEARCH ARTICLE
10.1002/2014TC003723

Key Points:
- New data from 4-D analog experiments
- Two-phase tectonic evolution to generate structures similar to the ESFZ
- Initial extensional phase related with a slab rollback process

Supporting Information:
- Readme
- Table S1 and Figures S1–S6
- Video S1
- Video S2
- Video S3
- Video S4
- Video S5
- Video S6
- Video S7
- Video S8
- Video S9

Correspondence to:
J. Alonso-Henar,
jahenar@geo.ucm.es

Citation:
Alonso-Henar, J., G. Schreurs, J. J. Martinez-Díaz, J. A. Álvarez-Gómez, and P. Villamor (2015), Neotectonic development of the El Salvador Fault Zone and implications for deformation in the Central America Volcanic Arc: Insights from 4-D analog modeling experiments, *Tectonics*, *34*, 133–151, doi:10.1002/2014TC003723.

Received 29 AUG 2014
Accepted 25 DEC 2014
Accepted article online 7 JAN 2015
Published online 29 JAN 2015

Neotectonic development of the El Salvador Fault Zone and implications for deformation in the Central America Volcanic Arc: Insights from 4-D analog modeling experiments

Jorge Alonso-Henar[1,2], Guido Schreurs[3], José Jesús Martinez-Díaz[1,4], José Antonio Álvarez-Gómez[1], and Pilar Villamor[5]

[1]Universidad Complutense de Madrid, Geodynamics, Madrid, Spain, [2]CEI Campus Moncloa, UCM-UPM, Madrid, Spain, [3]Institute of Geological Sciences, University of Bern, Bern, Switzerland, [4]Instituto de Geociencias (UCM, CSIC), Madrid, Spain, [5]GNS Science, Lower Hutt, New Zealand

Abstract The El Salvador Fault Zone (ESFZ) is an active, approximately 150 km long and 20 km wide, segmented, dextral strike-slip fault zone within the Central American Volcanic Arc striking N100°E. Although several studies have investigated the surface expression of the ESFZ, little is known about its structure at depth and its kinematic evolution. Structural field data and mapping suggest a phase of extension, at some stage during the evolution of the ESFZ. This phase would explain dip-slip movements on structures that are currently associated with the active, dominantly strike slip and that do not fit with the current tectonic regime. Field observations suggest trenchward migration of the arc. Such an extension and trenchward migration of the volcanic arc could be related to slab rollback of the Cocos plate beneath the Chortis Block during the Miocene/Pliocene. We carried out 4-D analog model experiments to test whether an early phase of extension is required to form the present-day fault pattern in the ESFZ. Our experiments suggest that a two-phase tectonic evolution best explains the ESFZ: an early pure extensional phase linked to a segmented volcanic arc is necessary to form the main structures. This extensional phase is followed by a strike-slip dominated regime, which results in intersegment areas with local transtension and segments with almost pure strike-slip motion. The results of our experiments combined with field data along the Central American Volcanic Arc indicate that the slab rollback intensity beneath the Chortis Block is greater in Nicaragua and decreases westward to Guatemala.

1. Introduction

The El Salvador Fault Zone (ESFZ) is a segmented strike-slip fault zone with a dominant N90°E–N100°E trend located in central El Salvador (Figure 1). This fault zone is situated in the Central America Volcanic Arc (CAVA) near the western limit of the Chortis Block within the Caribbean plate [*Martinez-Diaz et al*., 2004]. Although several studies have described the geometry and present-day kinematics of the ESFZ [*Martinez-Diaz et al*., 2004; *Corti et al*., 2005a; *Agostini et al*., 2006; *Canora et al*., 2010, 2012], few studies have dealt with its development and evolution. Recent studies by *Canora et al*. [2014] using structural field data, Digital Elevation Model (DEM), and satellite image analysis, and by *Alonso-Henar et al*. [2014], using morphometric analyses of relief suggest that part of the structures are better explained by an extensional tectonic regime rather that the current strike-slip dominated tectonic regime in the ESFZ. Both studies conclude that an extensional phase previous to the current tectonic regime is required to explain the overall structure of the ESFZ. They suggest that the extensional phase is related to slab rollback of the Cocos Plate beneath the Chortis Block, a process that was first proposed for Western Nicaragua by *Weinberg* [1992]. Such a possible evolution leads to some open questions that we address in our research: Does the ESFZ form during one phase of transtensional deformation, or do the structures in the ESFZ reflect a two-phase evolution, i.e., an early phase of extension overprinted by a later phase of strike slip or transtension? If the latter the case is correct, could extension have been caused by slab rollback beneath El Salvador?

Here we try to answer the questions above by using 4-D analog model experiments to test whether or not an extensional phase prior to the current strike-slip regime is required to obtain the overall, present-day geometry of the ESFZ. Analog modeling is an effective tool that allows us to control essential parameters (e.g., crustal thinning,

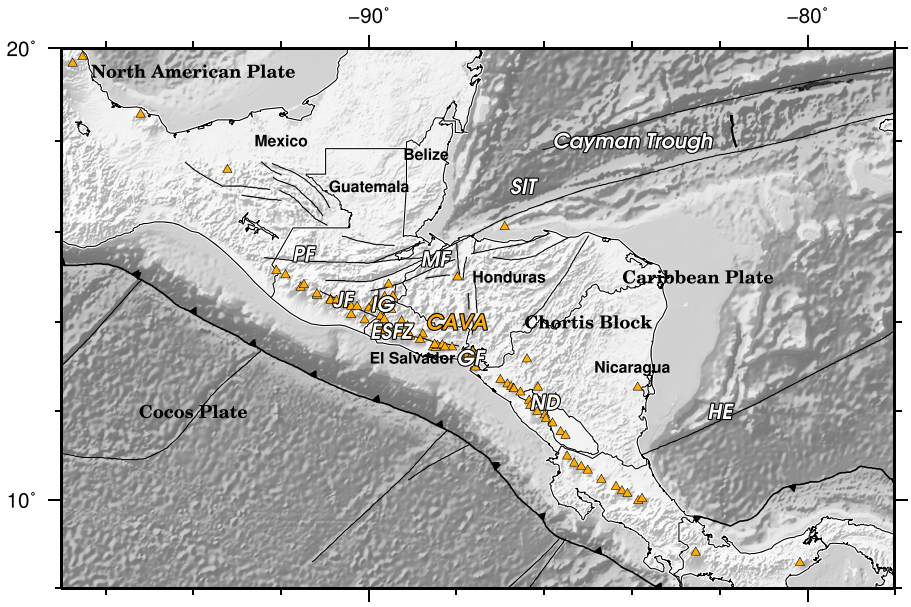

Figure 1. Tectonic setting of northern Central America. Orange triangles show the positions of volcanoes. Abbreviations are the following: SIT: Swan Island Transform Fault; PF: Polochic Fault; MF: Motagua Fault; JF: Jalpatagua Fault; IG: Ipala Graben; ESFZ: El Salvador Fault Zone; CAVA: Central America Volcanic Arc; GF: Gulf of Fonseca; ND: Nicaraguan Depression; HE: Hess Scarpment.

fault kinematic, and strain rates) that may disprove or confirm our hypothesis. To date, several experimental analog modeling studies have investigated: the influence of the orientation of the extension axis in distributed transtension [*Schreurs and Colletta*, 1998; *Schreurs*, 2003]; multiphase rift systems [*Keep and McClay*, 1997]; Riedel experiments, using a planar and vertical strike-slip basement fault [e.g., *Riedel*, 1929; *Tchalenko*, 1970; *Naylor et al.*, 1986; *Burbidge and Braun*, 1998]; and the relationship between volcanism and strike-slip tectonics [*Corti et al.*, 2005b; *Mathieu and van Wyk de Vries*, 2011; *van Wyk de Vries and Matela*, 1998]. While these studies bring light into some aspects of our study, they do not fully help answering the specific questions posed here for the ESFZ. Therefore, we have designed sandbox experiments to model the ESFZ structures to address alternative models and compared results with published models.

The results of this study are relevant for an appropriate modeling of fault sources for seismic hazard assessment in the region. Our results also contribute to the understanding of the evolution of the western plate boundary of the Caribbean plate in Central America.

2. Tectonic Setting

The ESFZ is located in the western margin of the Chortis Block, a crustal block composed of Paleozoic basement, Mesozoic marine sedimentary rocks, and Cenozoic rocks of the CAVA (Figure 1) [*Wadge and Burke*, 1983; *Pindell and Barret*, 1990; *Rogers et al.*, 2002]. The CAVA formed as a consequence of subduction of the Cocos plate beneath the Chortis Block and extends from Costa Rica to Guatemala, where it ends abruptly at the Polochic Fault. Trenchward migration of the CAVA is suggested by the relative location of volcanism in Nicaragua and in El Salvador; currently active volcanoes are located closer to the trench compared to the Miocene volcanoes [*Bundschuh and Alvarado*, 2007]. The CAVA can be divided into three zones based on structural style and geomorphology within the volcanic front [*Álvarez-Gómez*, 2009]. From southeast to northwest these zones are the following: the Nicaraguan Depression, extending from Northern Costa Rica to the Gulf of Fonseca [*McBirney and Williams*, 1965; *van Wyk de Vries*, 1993]; the ESFZ, crossing El Salvador from the Gulf of Fonseca to approximately the Gualtemala-El Salvador border [*Stoiber and Carr*, 1973; *Rose et al.*, 1999; *Martinez-Diaz et al.*, 2004]; and the Jalpatagua Fault that disappears northwestward in Guatemala [*Muehlberger and Ritchie*, 1975; *Carr*, 1976] (Figure 1).

The northern boundary of the Chortis Block is the Motagua-Polochic-Swan Island transform fault (northern boundary of the Caribbean plate), a fault zone with pure left-lateral strike-slip motion. The interaction

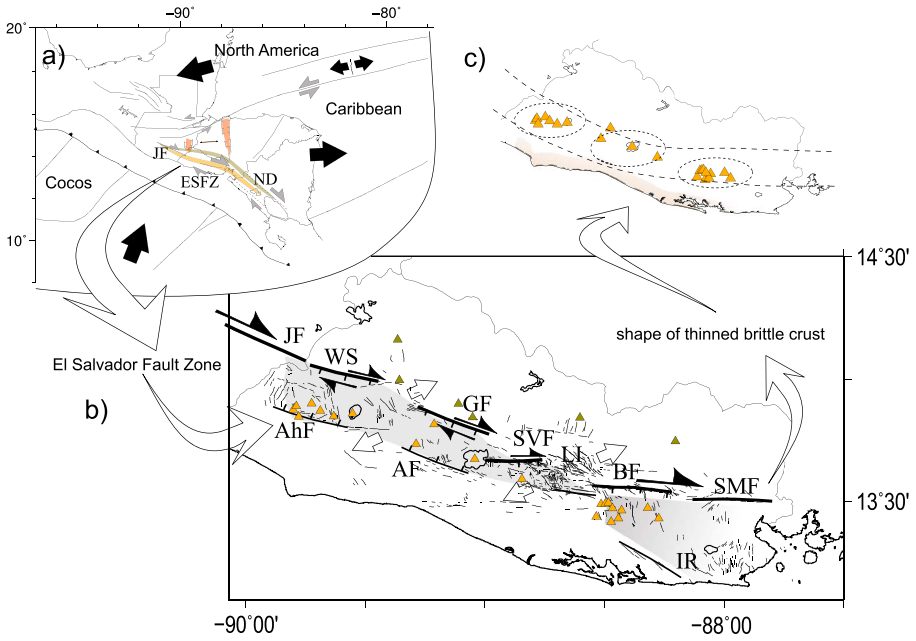

Figure 2. (a) Plate and relative motions of crustal blocks and main tectonic structures within Northern Central America, modified from *Álvarez-Gómez* [2009]. North America fixed. JF: Jalpatagua Fault; ESFZ; El Salvador Fault Zone; ND: Nicaragua Depression. (b) Main structures of the El Salvador Fault Zone [after *Canora et al.*, 2012]. Green triangles are Miocene volcanoes, and orange triangles are Pleistocene volcanoes. JF: Jalpatagua Fault; WS: Western segment; AhF: Ahuachapan Fault; GF: Guaycume Fault; AF: Apaneca Fault; SVF: San Vicente Fault; LI: Lempa Intersegment Zone; BF: Berlin Fault; SMF: San Miguel Fault; IR: Intipucá Range. Thin black lines are faults. Thick black lines are faults with large escarpments (ticks indicate the downthrown side). (c) Location of major volcanism and definition of the geometry of the continuous and discontinuous crustal weak (thinned brittle crust) zones used in the experimental procedure.

between the Caribbean, North American, and Cocos plates results in a diffuse triple junction in Guatemala, where the deformation is distributed in a broad area [i.e., *Plafker*, 1976; *Guzman-Speziale et al.*, 1989; *Guzman-Speziale and Meneses-Rocha*, 2000; *Lyon-Caen et al.*, 2006; *Authemayou et al.*, 2011] (Figure 1).

The El Salvador Fault Zone is a 150 km long and 20 km wide deformation zone within the Salvadorian part of the CAVA [*Martinez-Diaz et al.*, 2004; *Corti et al.*, 2005a]. The ESFZ consists of major strike-slip faults trending N90°E–N100°E that concentrate most of the displacement, and secondary normal faults trending between N120°E and N170°E. From northwest to southeast the most important faults are the following: Western segment, Ahuachapan Fault, Guaycume Fault, Apaneca Fault, San Vicente Fault, Lempa intersegment, Berlin Fault, and San Miguel Fault (Figure 2). The Jalpatagua Fault forms the along-strike continuation of the ESFZ to the northwest. The along-strike continuation toward the southeast is less clear, and the ESFZ disappears at the Gulf of Fonseca (Figure 2).

The ESFZ deforms the Quaternary alluvial deposits ignimbrites and pyroclastic flows of the Tierra Blanca Joven and Cuscatlan Formations with right-lateral displacement along its main segments [*Martinez-Diaz et al.*, 2004; *Corti et al.*, 2005a]. Horizontal offsets of Holocene deposits and of the drainage network can reach up to 200 m [*Corti et al.*, 2005a; *Canora et al.*, 2012]. Recent GPS and earthquake focal mechanism analysis suggest that strike-slip motion is predominant along the ESFZ and that the transtensional component is small [*Canora et al.*, 2010; *Staller*, 2014]. However, some of the present-day tectonic and geomorphic features of the El Salvador Fault Zone cannot be explained with the current strike-slip dominated tectonic context [*Alonso-Henar et al.*, 2014; *Canora et al.*, 2014]. These include the presence of active strike-slip faults with associated fault scarps up to 300 m and a dip of 70°, and graben-like structures (Figure 2).

3. Description of the Hypothesis

Weinberg [1992] described the neotectonic development of western Nicaragua and distinguished three deformation phases during the upper Miocene to Holocene. The first deformation phase (Miocene to early

Pliocene) is characterized by a lower subduction zone dip angle and a higher mechanical coupling of the Cocos and Caribbean plates interface. During this stage, the shortening was perpendicular to the trench, and the maximum horizontal stress (Shmax) was trending toward NE causing NW-SE folding. The second phase (upper Pliocene to Pleistocene) is characterized by NE-SW extension perpendicular to the trench. This phase is associated with an increase of the slab dip angle [*Weinberg*, 1992]. Rollback of the Cocos plate and mechanical decoupling of the Cocos and Caribbean plates are interpreted to have caused the Nicaraguan Depression, together with seaward migration of the volcanic front. *Weinberg* [1992] related the slab rollback to a decrease of the convergence rate between the Cocos plate and Chortis Block previously described by *Jarrard* [1986]. The third and current phase (middle Pleistocene to Holocene) generated strike-slip faults, pull-apart basins, and the Managua Graben.

The active volcanic front in Nicaragua has a position nearer to the trench than the Miocene volcanic arc [*Bundschuh and Alvarado*, 2007; *Weinberg*, 1992] (Figure 2a). According to *Burkart and Self* [1985], in Guatemala inland Miocene volcanism is located 100 km to the north of the current volcanic front. These authors associate the migration of volcanism with the Ipala Graben formation and not with any slab process (Figure 1). In El Salvador, the active volcanic front is located 20 km south of the Miocene volcanic arc mapped in *Bundschuh and Alvarado* [2007]. Hence, it is reasonable to hypothesize that subduction rollback of the Cocos plate also occurred beneath El Salvador. Moreover, it is also possible that the fault scarps along the strike-slip faults and graben-like structures along the volcanic front could also have formed during extension related to the rollback process.

The segmentation of the CAVA has influenced the structural style [*Stoiber and Carr*, 1973; *Burkart and Self*, 1985; *Agostini et al*., 2006; *Morgan et al*., 2008]. The position of the different magma chambers conditions crustal rheology and thereby could have determined the position of faults and the structural style [*Corti et al*., 2005b; *Mazzarini et al*., 2010; *Mathieu and van Wyk de Vries*, 2011]. For example, based on geochemical data *Agostini et al*. [2006] proposed three large weak areas that represent three independent large magma chambers in the Salvadorian volcanic front. According to these authors, these weak areas could have driven the segmentation of the ESFZ with formation of three E-W strike-slip faults with extensional step overs and related pull-apart basins. They also concluded that the active volcanism is confined to the three segments and almost inexistent in the pull-apart basins.

The larger E-W oriented strike-slip faults described by *Martinez-Diaz et al*. [2004] are consistent with the conclusions by *Agostini et al*. [2006]. However, *Canora et al*. [2014] noticed that the San Vicente, Ahuachapan and Apaneca Faults, and the Western Segment have associated fault scarps and tectonic depressions that cannot be explained purely by the Quaternary right-lateral strike-slip motion identified by *Corti et al*. [2005a] and *Canora et al*. [2012] (Figure 2). *Alonso-Henar et al*. [2014] quantified the active extensional component along the ESFZ and concluded that the Quaternary strain regime cannot generate some of these fault scarps and that a previous extensional phase is necessary to produce these morphologies. Several major E-W faults of the ESFZ are dipping 70° [*Canora et al*., 2010], which would be unusual for neoformed strike-slip faults. Quaternary motion of ESFZ reveals some transtensional strain, but this strain is not enough to explain the whole structure of the ESFZ. *Canora et al*. [2014] propose a model for the development of the ESFZ, consisting of an extensional phase that generated E-W oriented grabens along the volcanic front, and a later transtensive deformation phase that linked those grabens through strike-slip faults. Reactivation of the normal faults of the graben as strike-slip faults could explain the present fault scarps of the San Vicente, Ahuachapan, Apaneca Faults, and the Western segment of the ESFZ.

4. Experimental Procedure

We have carried out a series of experiments combining transtension, strike slip, and extensional tectonics to investigate the formation and evolution of structures in the ESFZ. In our experiments we used different model geometries to simulate weaker (thinned) continental crust of the volcanic arc formation associated with slab rollback of the Cocos plate beneath the Chortis block. We model the weaker continental crust either by a continuous thinned zone or a discontinuous thinned zone (Figures 2 and 3). Our experimental setups are inspired by strike slip and transtensional experiments done by *Schreurs and Colletta* [1998] and multiphase rift experiments done by *Keep and McClay* [1997].

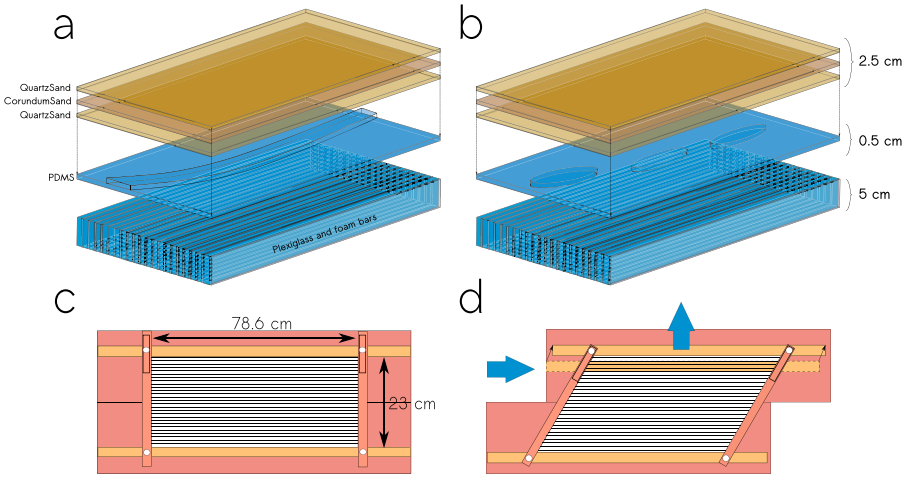

Figure 3. Experimental setup. (a) Continuous crustal thinning, (b) discontinuous crustal thinning, and (c and d) modeling apparatus prior and after deformation. PDMS: Polydimethylsiloxane.

4.1. Analog Materials and Model Scaling

We used granular materials and viscous materials to simulate the brittle behavior of the upper crust and the ductile behavior of the lower crust, respectively. As granular materials we used quartz sand and brown corundum sand with a grain size range of 80–200 μm and 88–125 μm and bulk densities of 1.56 g cm^{-3} and 1.89 g cm^{-3}, respectively. Quartz and corundum sand have similar mechanical properties with internal friction angles between 35° and 37° [*Panien et al.*, 2006], similar to values obtained for upper crustal rocks by *Byerlee* [1978]. As viscous material we used Polydimethylsiloxane (PDMS) with a density of 0.965 g cm^{-3} and a viscosity value in the Newtonian regime of 5×10^4 Pa s [*Weijermars*, 1986]. PDMS is considered to be a good analog material to model viscous flow of lower crustal rocks [*Vendeville et al.*, 1987]. However, it has its limitations as an analog of the lower crust because its density is lower than the overlying brittle material. In our experimental setup, the PDMS is placed at the base of the model and distributes the imposed deformation evenly over the entire width of the model and prevents the localization of deformation.

It is necessary to establish scale ratios between model and natural prototype (expressed by the superscript asterisk). The length ratio of our experiments is $L^* = 2 \times 10^{-6}$ (implying that 1 cm in the model represents 5 km in nature). The density ratio for the quartz sand is $\rho^* = 0.6 \pm 0.08$ and for the corundum sand is $\rho^* = 0.73 \pm 0.09$, assuming values for the upper crust that range between 2.3 and 3.0 g cm^{-3}. The experiments were carried out under normal gravity, and $g^* = 1$. The viscosity ratio is $\eta^* = 2.5 \times 10^{-16}$ Pa s considering a viscosity for the lower ductile crust of 2×10^{20} Pa s.

The strain rate is different in each model but lies within the same order of magnitude (10^{-6} s^{-1}). Considering that the velocity ratio is $V^* = \dot{e}^* \times L^*$, with $\dot{e}^*$ the strain rate and assuming natural strain rates between 10^{-15} and 10^{-13} s^{-1} [*Pfiffner and Ramsay*, 1982]. The applied velocities in the models are equivalent to approximately 30 mm/yr of strain rates in nature, which is close to the GPS velocity values obtained by *DeMets et al.* [2010], for the studied tectonic context. The experimental parameters are summarized in Table 1.

4.2. Modeling of Volcanic Arc Region Within Weaker Continental Crust

Active volcanic arcs have a high thermal gradient with the 300–400°C isotherms, which brings the brittle-ductile transition to a shallower level than in standard continental crust [*Scholz*, 2002]. In case of the Taupo Volcanic Zone in New Zealand, the brittle-ductile transition is at approximately 6 to 10 km depth [*Bryan et al.*, 1999], based on seismicity data. *Hasegawa et al.* [2000] show that this depth is variable along the volcanic arc in Japan with a maximum depth of 14 to 15 km and a minimum depth of 10 km in the areas with active volcanoes. In the Mexican volcanic belt, *Ortega-Gutiérrez et al.* [2008] calculated a thermal gradient between 27 and 57°C km^{-1} implying a brittle crustal thickness varying between 15 and 7 km (using 400°C). In El Salvador,

Table 1. Parameters of Analog Models

Experiment No.	Nature of Weak Zone	Kinematics	Initial Model Dimension (mm)	Total Extension of Sidewalls (mm)	Total Movement of the Base Plate (mm)	Ductile Layer Thickness (cm)	Brittle Layer Thickness (cm)
435	Continuous	Strike slip	230 × 786	0	80	0.5 or 1	2.5 or 2
438	Discontinuous	Strike slip	230 × 786	0	80	0.5 or 1	2.5 or 2
444	Continuous	Extension + strike slip	230 × 786	8	51	0.5 or 1	2.5 or 2
443	Discontinuous	Extension + strike slip	230 × 786	5.5	70	0.5 or 1	2.5 or 2
446	Continuous	Transtension	230 × 786	22	54	0.5 or 1	2.5 or 2
445	Discontinuous	Transtension	230 × 786	22	54	0.5 or 1	2.5 or 2
447	Continuous	Extension + transtension	230 × 786	28	49	0.5 or 1	2.5 or 2
448	Discontinuous	Extension + transtension	230 × 786	26	49	0.5 or 1	2.5 or 2

Canora et al. [2010] proposed a brittle crustal thickness of 10 km based on seismotectonic analysis of the 13 February 2001 earthquake and its aftershock sequence.

To test the influence of a broad zone of crustal thinning in possible association with slab rollback, we modeled a continuous area of thinned brittle crust with a concave-to-the-north geometry similar to the shape of the Salvadorian volcanic arc (Figures 2 and 3a). The width of this area of 20 km is defined by the distance between the Miocene and the Pleistocene-Holocene volcanic arc in El Salvador. This width is modeled by a 4 cm wide strip of thinned brittle crust in the experiments. The thickness of the brittle crust in the experiments is 2 cm in the thinned region and 2.5 in the surrounding areas corresponding to 10 km and 12.5 km in nature, respectively. To test the influence of a thinned brittle crust in association with large magma chambers, as proposed by *Agostini et al.* [2006], we modeled a discontinuous thinned brittle crust simulating three segmented zones of the volcanic arc, acting as weakness zones (Figures 2b, 2c, and 3b).

4.3. Experimental Setup

The experimental apparatus consists of two base plates that can move laterally past one another and two longitudinal sidewalls. Computer-driven servomotors control the relative movements of the sidewalls and base plates. The initial dimension of each model is 78.8 (length) × 23 (width) × 3 cm (height). The base and longitudinal walls are made of carbon fiber and wood, respectively, whereas the transverse boundaries of the model are confined by elastic rubber sheets (Figures 3c and 3d).

To simulate extension and transtension we used a similar setup as the one used by *Schreurs and Colletta* [1998]. On top of the two base plates and between the sidewalls we stacked 35 bars 5 cm high and 78.8 cm long; 18 plexiglass bars each 0.5 cm wide alternating with 17 foam bars each 1 cm wide. Before constructing the model, the sidewalls were displaced compressing the bars from 26 to 23 cm wide, the initial width of the model. By extending the longitudinal sidewalls after the model has been constructed, the foam bars decompress and extensional strain is distributed across the entire model. The distributed strike-slip component in transtension experiments is induced by moving one of the base plates, resulting in lateral slip of each bar. Pure strike-slip experiments were done using 46 plexiglass bars each 0.5 cm wide, 5 cm high, and 78.8 cm long between the sidewalls of the apparatus. The movement of one of the base plates induces lateral slip between the plexiglass bars causing distributed strike slip (Figures 3c and 3d).

The changes of thickness in the PDMS layer reflect the desired brittle crustal thickness. A 0.5 cm to 1 cm thick layer of PDMS was placed over the foam and plexiglass bars. The thicker areas of PDMS represent the thinner areas of the brittle layer, and the location and shape of the weak zones, either continuous or discontinuous. The PDMS layer distributes the imposed shear evenly over the entire model and avoids localization of deformation above the discontinuities generated between adjacent plexiglass bars. Directly on top of the PDMS layer we sieved two quartz sand layers with an interbedded corundum sand layer, with a total maximum thickness of 2.5 cm (Figure 3).

All experiments, except two (experiments 335 and 338), were analyzed by X-ray computed tomography (XRCT), a nondestructive technique that allows us to analyze in detail the evolution of the 3-D geometry of structures with time [*Schreurs et al.*, 2003]. In addition, surface photographs were taken at regular time steps.

Table 1. (continued)

Max Shear Strain (γ)	Extension Velocity (mm/h)	Base Plate Velocity (mm/h)	Extension Strain Rate (s^{-1})	Shear Strain Rate (s^{-1})	Figure No.
0.35		20		2.4×10^{-5}	Figures 4a–4d
0.35		20		2.4×10^{-5}	Figures 4f–4i
0.21	9.4	20.7	1.1×10^{-5}	2.4×10^{-5}	Figures 5a–5c
0.30	12	20.3	0.9×10^{-5}	1.7×10^{-5}	Figures 5d–5g
0.21	7.3	18	0.8×10^{-5}	1.9×10^{-5}	Figures 6a–6c
0.21	7.5	18.5	0.9×10^{-5}	2.0×10^{-5}	Figures 6d–6f
0.19	First phase 7.9 Second phase 7.3	Second phase 18	First phase 1.0×10^{-5} Second phase 0.7×10^{-5}	1.9×10^{-5}	Figures 7a–7c
0.19	First phase 9.4 Second phase 7.4	Second phase 18	First phase 1.1×10^{-5} Second phase 0.4×10^{-6}	2.0×10^{-5}	Figures 7d–7g

5. Model Results

To test different geodynamical scenarios, we carried out experiments with the following kinematic constrains (Table 1): (a) a single strike-slip phase, (b) an extensional phase followed by a strike-slip phase, (c) a single transtensional phase (divergence direction (β) approximately 22°, with $\beta = \tan^{-1}$ (extension/shear)), and (d) an extensional phase followed by a transtensional phase (divergence direction (β) approximately 22°). Each of these scenarios was tested for model runs with either a continuous or a discontinuous weak zone. The weak zone represents an area where the viscous layer is thicker and the overlying brittle layer is thinner than in the rest of the model, hence simulating a region of thinned brittle crust in nature. All experimental parameters of the models are given in Table 1.

5.1. One Phase of Strike Slip

Experiments 435 and 438 (Figure 4) test whether pure dextral strike slip can generate structures similar to those observed in the ESFZ.

Experiment 435 (Continuous Weak Zone. Figures 4a–4d). During the early stages of the experiment ($\gamma = 0.06$; Figure 4a), left-stepping, en echelon dextral faults form above the weak zone striking at 25° to 30° (all surface strikes are given with respect to the longitudinal sidewalls). These faults correspond to synthetic Riedel shears (R) [see, e.g., *Naylor et al*., 1986; *Schreurs*, 2003]. In the region where the weak zone strikes at higher angles (>10°) to the longitudinal sidewalls, R shears are longer and relays are less clear. With progressive deformation, R shears in the left side of the model link up to form a through-going fault zone (Figure 4b). In the region where the weak zone is parallel to the longitudinal sidewalls individual, en echelon R shears only develop after some deformation ($\gamma = 0.13$; Figure 4b). R shears and some splay faults (S) [see *Naylor et al*., 1986] are still clearly visible at $\gamma = 0.13$ (Figure 4b). At a shear strain of $\gamma = 0.22$, new dextral shear faults striking at 10° to 15° link up with previously formed faults (Figure 4c). A graben with faults striking at 20° forms in the region where the thinned brittle crust changes its strike from 30° to 0°. In the right side of the model, new dextral faults striking at approximately 0° offset and link earlier formed dextral faults resulting in an anastomosing fault zone (L in Figures 4c and 4d). During the late stages of the experiment, reverse faults and strike-slip faults form in the acute corners of the model reflecting boundary effects.

Experiment 438 (Discontinuous Weak Zone. Figures 4e–4h). In this experiment the structure and its evolution are linked to the presence of the individual weak zones. As in the previous experiment, the first faults to appear are R shears striking at 25° (Figure 4e) but they form in correspondence to discontinuous weak zones. With increasing deformation ($\gamma = 0.11$), R shears link up resulting in two well-developed dextral fault zones that form a restraining step over with a pop-up structure in the central part of the model (Figure 4g). Sinistral strike-slip faults striking at 75° (antithetic R shears) form in the left side of the model, and new dextral faults form crosscutting and linking the pop-up structure. At advanced stages of the experiment ($\gamma = 0.35$; Figure 4h), the push-up structure becomes inactive and P and R shears offset the structure. Two grabens striking at 20° form on either side of the pop-up structure. Sinistral strike-slip faults, corresponding to R_l' shears of *Schreurs* [2003], form in between overlapping dextral strike-slip fault zones. In the lateral parts of the model, reverse faults related to boundary effects are frequent.

5.2. Extension Followed by Strike Slip

Experiments 444 and 443 (Figure 5) are multiphase experiments, consisting of a pure extensional phase followed by a pure dextral strike-slip phase.

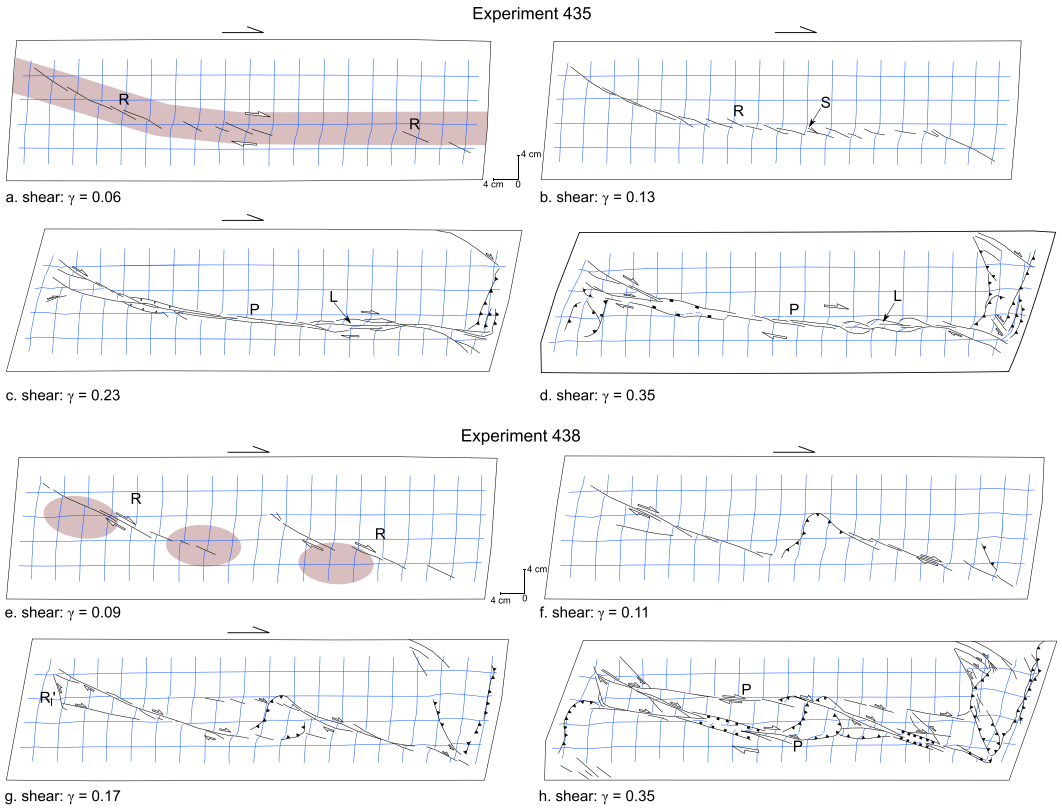

Figure 4. (a–h) Experiments 435 and 438: strike slip. Grey areas indicate the initial outline of the weak zone (thinned brittle crust).

Experiment 444 (Continuous Weak Zone. Figures 5a–5c. XRCT Cross Sections in Supporting Information Figure S1). During the extension phase, an almost continuous graben forms above the weak zone. The normal faults bounding the graben have a dip of approximately 70°. The graben forms first above the weak zone that strikes perpendicular to the extension direction. It propagates along-strike curving into the weak zone striking at an angle. Small relays form during graben formation (Figure 5a and supporting information Video S1. This Video S1 consists of contiguous XRCT cross sections taken from right to left.)

During the second phase, normal faults are reactivated as dextral strike-slip faults. In addition, new strike-slip faults striking at approximately 0–10° form within the graben and link up both sides of the graben. A right-lateral strike-slip fault offsetting the graben is generated in the left side of the model above the limit of the weak zone (fault N in Figures 5b and 5c). There are some boundary effects near the acute corners of the model (Video S2).

Experiment 443 (Discontinuous Weak Zone. Figures 5d–5g and XRCT Cross Sections in Figure S2). During the extensional phase, grabens form above the three weak zones striking perpendicular to the extension direction. The grabens propagate along strike away from the weak zones and overlap partially. Graben-bounding faults have dip angles of 70°.

Similar to the previous experiment, graben-bounding faults are reactivated as pure dextral strike-slip faults during the second phase of deformation. In the intersegment zones (diffuse deformation areas), new faults appear and link the grabens produced during the first phase (Figure 5f). With increasing deformation, new dextral strike-slip faults with complex geometries and striking at low angles form within grabens or connect segmented grabens. Some of these strike-slip faults link oppositely dipping graben-bounding faults and change their dip direction 180° along strike (Figures 5f and 5g and Videos S3 (stage 1) and S4 (stage 3)). The structural complexity of intersegment zones (the areas between thinned brittle crust) increases with increasing strike-slip deformation. The intersegment areas are characterized by fault relays and complex faults with variable dip and dip direction (Figures 5d–5g and Figure S2).

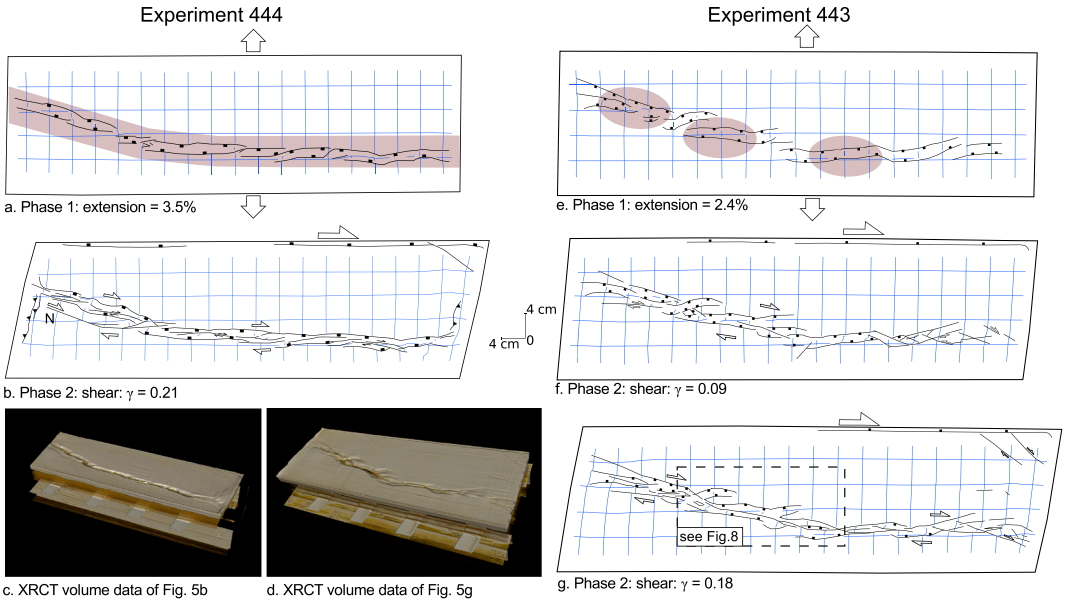

Figure 5. Multiphase experiments 443 and 444: extension followed by pure strike slip. (a–c) Experiment with continuous weak zone and (d–g) experiment with discontinuous weak zone. Perspective views constructed from XRCT data are shown for experiment 444 (Figure 5c) and experiment 443 (Figure 5d). Dashed rectangle shows the location of the detail shown in Figure 8.

5.3. One Phase of Transtension

Experiments 445 and 446 (Figure 6) test whether one phase of dextral transtension can explain the complex fault geometry of the ESFZ. The angle of divergence in both experiments is 22°.

Experiment 446 (Continuous Weak Zone. Figures 6a–6c and XRCT Cross Sections in Figure S3). In early stages of dextral transtension, dextral strike-slip faults form above the weak zone with a 30° to 40° trend in the left side and a 10° to 20° trend in the central right side of the model. A series of antithetic strike-slip faults form in the left side of the model. Also, in the left side of the model, the early formed dextral strike-slip faults acquire a component of normal slip leading to the development of a graben (Figure 6a). With progressive deformation, this graben propagates along strike and changes its strike direction mimicking the shape of the weak zone. With increasing transtension, the graben becomes deeper and continuous all along the weak zone. In the right side of the model, some strike-slip faults remain active. A new 0° trending strike-slip fault forms at advanced stages of transtension (fault N in Figures 6c and S3 and Video S5). As the strain increases, boundary effects become apparent in the acute corners of the model.

Experiment 445 (Discontinuous Weak Zone. Figures 6d–6f and XRCT Scan Cross Sections in Figure S4). During the early stages of transtension, dextral strike-slip faults form in the right-side model. These faults acquire a normal-slip component with continuing transtension, and they form graben. Major dextral strike-slip faults appear in the left side of the model, and antithetic faults appear in the central-left side of the model (Figures 6d and 6e). Dextral strike-slip faults dip at 85–90°, and the graben-bounding faults dip at 70°. The graben and dextral strike-slip faults strike at 20°. There is an area of diffuse deformation between the graben and the main fault of the left side of the model (between weak zones 2 and 3). In this area, an array of sinistral strike-slip faults form (R_I' of *Schreurs* [2003]). Their dip angle decreases from subvertical to 70°. In the middle of the model, the activity of the R_I' shears stops, and the surrounding grabens connect and crosscut these faults. In the left and right sides of the model, new R_I' shears form that crosscut the graben. In the last stages of transtension (Figure 6f), a well-developed graben crosses the model, and 40–50° striking R_I' shears appear and offset the graben. Outside the main graben, R_I' shears also form that accommodate an important part of the transtension (Video S6).

5.4. Extension Followed by Transtension

Experiments 447 and 448 (Figure 7) simulate a phase of extension followed by a phase of transtension with a divergence angle of $\beta = 22°$.

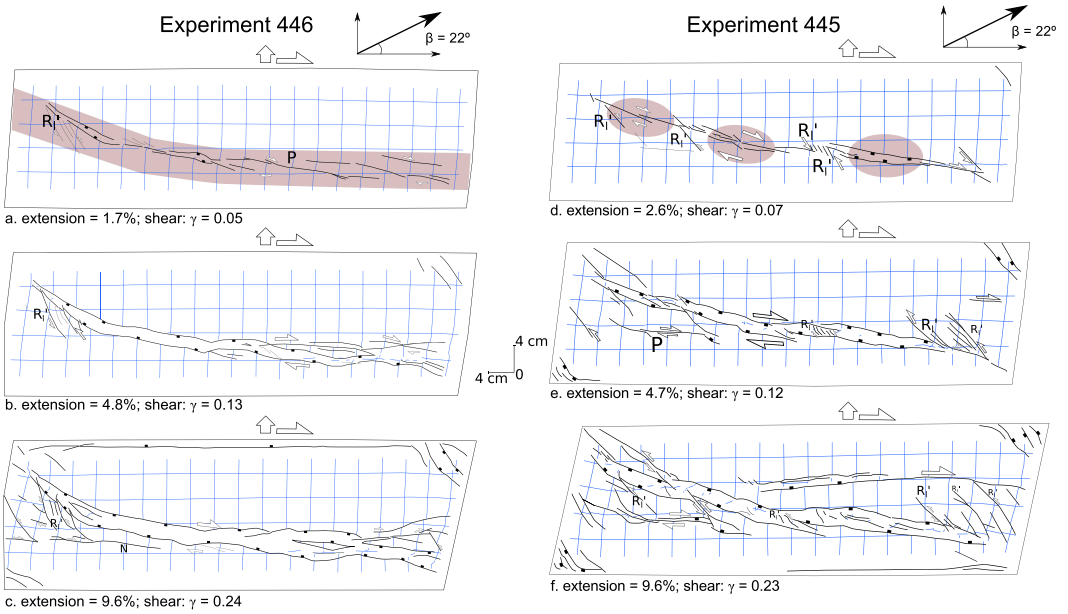

Figure 6. Single-phase transtension experiments (a–c) 446 with a continuous weak zone and (d–f) 447 with a discontinuous weak zone.

Experiment 447 (Continuous Weak Zone. Figures 7a–7c. XRCT Scan Cross Sections in Figure S5). The initial phase of extension shows similar fault patterns to experiment 444; at the end of the extensional phase, an almost continuous graben has formed above the weak zone (Figure 7a). The graben is slightly wider where the weak zone is oriented perpendicular to the extension direction. Relay structures form in the region where the orientation of the weak zone changes along strike.

During the transtensional phase ($\beta = 22°$), the graben-bounding faults are reactivated and a graben forms with a dextral strike-slip component. The orientation of the graben follows the geometry of the weak zone. Where the trend of the graben changes along strike (lower left side of model), a 0° trending dextral strike-slip fault extends from the graben to the left boundary of the model (fault N, in Figure 7b: this fault could be a boundary effect). Between this fault and the graben, antithetic strike-slip faults appear (as in experiment 446, Figure 6c). In the right side of the model, the deformation is accommodated by dextral strike-slip faults striking −10° and sinistral strike-slip faults striking 30°. The normal faults in the acute borders of the model are the result of boundary effects (see also Video S7 and Figure S5).

Experiment 448 (Discontinuous Weak Zone. Figures 7d–7g. XRCT Scan Cross Sections in Figure S6). The initial phase of extension has similar fault patterns to experiment 443 (Figures 5e–5g). During the early stages of deformation, grabens striking perpendicular to the extension direction form above the weak zones. Graben-bounding faults dip at 70° (Figure 7e and Video S8). With increasing extension, the grabens propagate along strike and overlap with each other. The lateral termination of each graben and step overs are closely coincident with the lateral extension of the weak zones. Minor faults near the longitudinal side wall are a boundary effect.

The structures inherited from the extensional phase control to a large extent the formation of the structures in the following transtensional phase. At the beginning of the transtensional stage, new faults striking at 30° link the graben structures in the intersegment zones between the grabens pull-apart basins are formed. The strike-slip component of the strain is accommodated inside the grabens where new strike-slip faults link both boundary faults of each inherited graben. Graben subsidence increases as the normal component of the grabens is still active (Figure 7f). As transtension progresses (Figure 7g), new R_I' shears appear striking at 30° to 40° and offsetting the grabens. At the same time, new dextral faults form with a trend parallel to and linking up with existing grabens. With continuing transtension, these faults propagate and acquire a dip-slip component resulting in the formation of grabens (Video S9).

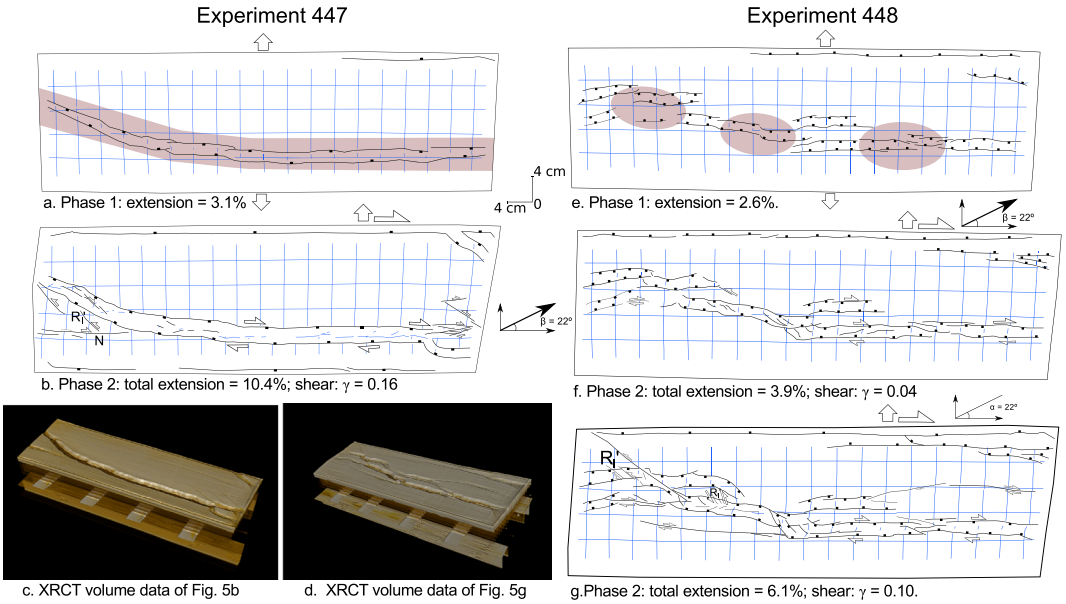

Figure 7. Multiphase experiments 447 and 448 modeling extension followed by transtension. (a–c) Experiment 447 has a continuous weak zone, and (d–g) experiment 448 has a discontinuous weak zone. Perspective views constructed from XRCT data are shown for experiments 447 (Figure 7c) and 448 (Figure 7d).

6. Discussion

Our experiments were constructed to better understand the structural evolution of the ESFZ. In particular, we have explored whether the structures of the ESFZ formed during one phase (of either strike slip or transtensional deformation) or whether the structures in the ESFZ are better explained with a two-phase evolutional model, i.e., an early phase of extension overprinted by a later phase of strike slip or transtension.

We divide this into three parts: First, we summarize structural aspects of strike-slip faulting and extensional-transtensional processes from our results and previous modeling studies; second, we compare our experimental results with the local and regional structure of the ESFZ structure with the aim to inform the structural evolution of the fault zone; and third, we discuss the geodynamical implications of our experimental studying the wider context of the plate boundary.

6.1. Inferences on Fault Patterns and Controls on the Structure From Analog Models

Models With a Continuous Weak Zone (Experiments 435, 444, 446, and 447). In models with a continuous weak zone, faulting localizes predominantly above this zone. In the single-phase strike-slip experiment (experiment 435), the fault pattern is dominated by en echelon strike-slip faults. With increasing shear, these faults connect but only limited graben formation occurs in the overlapping releasing segments. In the other three models, i.e., the one-phase transtensional model and the two multiphase models, a well-developed graben system forms. The curved shape of the weak zone results in along-strike differences in fault evolution, graben subsidence, and width. In the single-phase transtension experiment (experiment 446, $\beta = 22°$), graben formation starts above the oblique part of the weak zone (left side of the model), whereas strike-slip faults striking at low angles form initially above the remainder part of the weak zone. With increasing transtension, grabens propagate laterally from the oblique part until a through-going graben system forms. In both multiphase experiments (experiments 444 and 447) and after the extensional phase, the graben is narrower and shallower above the oblique part of the weak zone and wider and deeper above the remaining part of the weak zone. The existing graben faults acquire a strike-slip component during the second phase of deformation. In the case of a strike-slip second phase (experiment 444), new strike-slip faults form mostly within the existing graben as a result of local stress field modifications. It seems that the main principal stress rotates anticlockwise and becomes more parallel to the strike of the graben-bounding faults. In the case of a transtensional second phase (experiments 447), the graben-bounding faults are preferentially reactivated, and there is less intragraben faulting.

Models With a Discontinuous Weak Zone (Experiments 438, 443, 445, and 448). The fault evolution in models with a discontinuous weak zone is more complex than in models with a continuous weak zone. During initial deformation, faults form first above the discontinuous weak zones. In the single-phase experiments (experiments 438 and 445), dextral strike-slip faults initially form with strikes ranging between 25 and 30° for the pure strike-slip experiment (experiment 438) and between 15° and 20° for the transtension experiment (experiment 445). This difference in strike is clearly related to the extensional component of deformation in the transtension experiment and has also been documented by *Schreurs* [2003]. In contrast to the pure strike-slip experiment (experiment 438), the strike-slip faults in the transtension experiments (experiment 445) do acquire a dip-slip component with continuing deformation, which ultimately results in a major graben structure striking at approximately 15°. In pure strike-slip experiment (experiment 438), no graben structure forms, instead a pop-up structure forms between two major restraining fault segments. In the multiphase experiments (experiments 443 and 448), similar fault patterns appear by the end of the initial extensional phase. Also, in both experiments, a series of partially overlapping grabens strike perpendicular to the extension direction. The weak zones promote the development of a clearly segmented graben system during the first extension phase, which conditions the development of complex fault systems with local extension at the intersegment (intergraben) zones during the second phase of the model.

En Echelon Segmented Intragraben Faults and Strain Partitioning. *Keep and McClay* [1997] and *Bonini et al*. [1997] modeled polyphase rifting consisting of an orthogonal extensional phase and a later transtensional phase, albeit with a different experimental setup and without the presence of a weak zone. Both studies note that a minor part of the strike slip and extensional component is accommodated by en echelon faults formed during the oblique rifting stage. *Keep and McClay* [1997] showed that the first rifting phase exerts a major control on the subsequent structures that form during the second phase of transtensional deformation. Their experimental study suggests that segmentation of boundary faults, segmented en echelon intragraben faults, and salients and embayments in boundary faults are structures indicative of multiphase rifting. *Corti et al*. [2003] investigated the influence of a central weak zone in polyphase rift experiments. Their studies suggest that en echelon patterns during oblique rifting may be controlled by magma emplacements within the main rift depression. En echelon faults inside graben systems also appear in several of our experiments (experiments 444, 446, and 447; Figures 5–7). These en echelon faults drive a process of strain partitioning during the second phase of deformation. That is, when a branch of the graben is active, the opposite one is inactive, and the en echelon intragraben faults transfer the strain from one branch to the other one. The en echelon intragraben faults link the oppositely dipping faults of the graben system changing their dip direction along strike. In experiments by *Schreurs and Colletta* [1998], a similar phenomena can be observed in a transpressional regime. In those experiments, oppositely dipping thrusts of early formed pop-up structures are linked by strike-slip faults that change their dip direction along strike.

Intersegment Zones and Pull-Apart Basins. The first phase of the two multiphase experiments with a discontinuous weak zone (443 with a strike-slip second phase and 448 with a transtensional second phase) are identical (orthogonal extension), resulting in a segmented graben parallel to the long sides of the sand box. The segments preferentially form above the weak zones. Deformation during the second phase creates R shears and normal faults linking adjacent and partially overlapping grabens. Normal faults inherited from the first phase are reactivated as strike-slip faults or oblique slip faults.

While in experiment 443 (strike-slip second phase; Figures 5d–5g), the graben linkage during the second phase of strike-slip deformation is driven by R shears (with 20°–30° angles to the model walls), the linkage is achieved by fault with larger strikes (45–50°) in experiment 448 (transtensional second phase; Figures 7d–7g). The differences in strikes of linking faults of pull-apart basins are consistent with the studies done by *Wu et al*. [2009] on the influence of the transtensional angle during the development of a pull-apart basin. Although the second deformation phase in experiment 443 is pure strike slip, the partially overlapping grabens induce local transtension in the releasing dextral step overs, with the graben-bounding normal faults acting as strike-slip faults (Figure 8).

6.2. Comparison of Experimental Results With the El Salvador Fault Zone

We tried to reproduce some observations in the ESFZ in our analog models. The ESFZ is currently an almost pure strike-slip fault zone with minor transtension [*Staller*, 2014; *Canora et al*., 2014]. Some of the

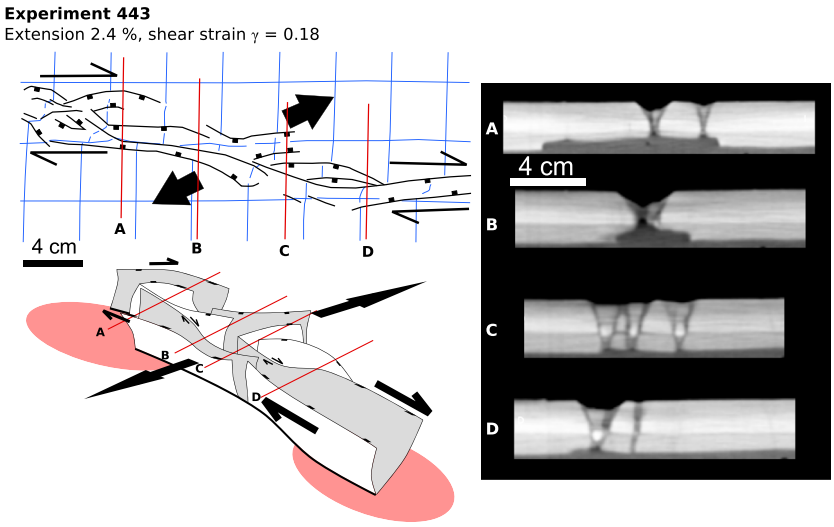

Figure 8. Detail of an intersegment zone of experiment 443. For location, see Figure 5g, dashed rectangle.

main strike-slip faults of the ESFZ have associated fault scarps up to 300 m high and dip angles of around 70°. Both observations cannot be explained within the current strike-slip dominated tectonic context. Some subtle graben structures have almost pure strike-slip faults bounding faults.

Our experimental results indicate that the experiment that best mimics the geometry of the ESFZ is experiment 443, with a discontinuous weak zone and a two-phase tectonic evolution, extension followed by pure strike slip (Figures 5d–5g and 9). In this model, the initial orthogonal extension generates independent grabens above the weak zones. During the second deformation phase (strike slip), the grabens are reactivated as strike-slip faults, and intergraben regions display a more diffuse deformation.

The fault pattern that forms in the early stages of phase 2 in experiment 443 (Figures 5f and 5g) is quite similar to the ESFZ fault pattern in a broad sense (Figure 9). However, there are also minor differences. The intersegment zones with local transtension along the ESFZ display secondary faults that are suborthogonal to the main segments and that were not reproduced in experiment 443. This could be due to the fact that only the northern fault of the graben-like structures of the ESFZ is being active and resulting in pull-apart basins. In contrast, during the second phase of pure strike-slip deformation in our model, both bounding faults of the graben are active, intragraben deformation develops, and the intersegment zones areas display diffuse deformation with faults linking the grabens.

Although the other multiphase experiment 448 with a discontinuous weak zone also reproduces first-order geometries observed in the ESFZ, it resembles the natural geometries less than experiment 443. However, it is interesting to note that in experiment 448 graben linkage occurs though normal faults that are suborthogonal to the graben structures and that are controlled by the transtensional strain during the second phase. In the ESFZ, some transtension could be present during the second phase promoting the development of the suborthogonal secondary faults. According to *Wu et al.* [2009], the geometry of pull-apart basins are controlled by the transtension angle, and small differences in the transtensional component control linkage of the main faults and hence the final geometry.

The multiphase experiment 444 with a continuous weak zone also shows first-order geometric similarities to the ESFZ (Figure 5b). However, in contrast to nature, a continuous graben is formed during the first extensional phase and intersegment zones are lacking. In addition, no local transtension is observed in the experiment during the second phase of pure strike slip.

By comparing models with a continuous and a discontinuous weak zone, we aimed to assess whether the location of grabens and normal faulting features is related to the presence of discontinuous weak zones. For example, *Agostini et al.* [2006] associated the presence of extensional features with the formation of pull-apart structures in between weak zones. *Agostini et al.* [2006] interpreted the ESFZ as the result of one phase of dextral strike-slip deformation in which three volcanic arc segments (weak zones) determine the

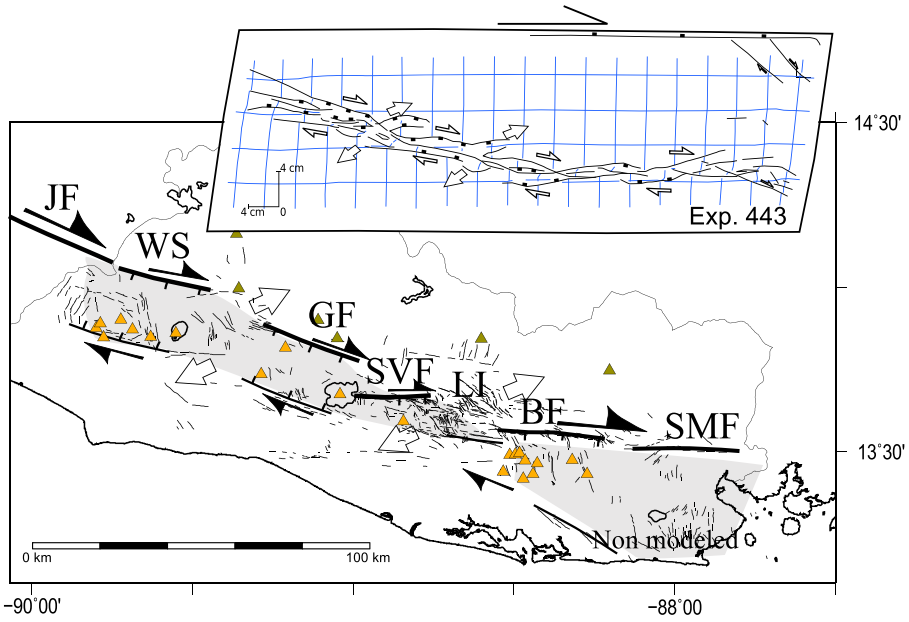

Figure 9. Comparison between experiment 443 (stage 3) and the ESFZ. Same abbreviations as in Figure 2. Half arrows indicate the strike-slip movement of the graben-bounding faults. Full arrows indicate local transtension located in the intersegment zones, both in the model and in the structural map.

location of the main segments of the ESFZ. They suggested that a major E-W dextral strike-slip fault developed over each volcanic arc segment resulting in right-stepping strike-slip fault system. Pull-apart basins, with extensional features, are inferred to have formed between the releasing step overs of the main segments (Figure 10a). Experiment 438 (discontinuous weak zone and one phase of pure strike slip; Figures 4e–4h) was run to investigate the hypothesis of *Agostini et al*. [2006]. Our results differ significantly from the model proposed by *Agostini et al*. [2006]. In experiment 438 (Figures 4e–4h), two R shears appear with a push-up structure developing between them (Figure 10b). The fact that the results of the experiment 438 differ from *Agostini et al.*'s [2006] conceptual model may stem from the setup and the rheology of our experiments. This can be inferred from comparisons with other analog models. For example, *Corti et al*. [2005b], modeled magma intrusions during strike-slip experiments using a simple shear deformation apparatus. In their models strike-slip faults parallel to the shear direction were formed. In experiments by *Holohan et al*. [2008] simulating caldera collapse in a strike-slip tectonic regime, they note that prior to caldera collapse restraining structures are formed and that faults are not parallel to the displacement direction. We suggest that the model setup used by *Corti et al*. [2005b] and *Holohan et al*. [2008], together with the viscous material used to simulate ductile crust, controls the degree of coupling with the basal plates and controls whether or not strike-slip faults form parallel to the displacement direction. A weaker ductile crust together with a simple shear apparatus promote the development of segments over the discontinuities and the development of pull-apart basins in the intersegment zones as proposed by *Agostini et al*. [2006] (Figure 10a).

Stoiber and Carr [1973] and *Agostini et al*. [2006] highlight the existence of well-developed volcanic segments in the ESFZ with monogenetic volcanoes in the intersegment areas. From the results of our experiments, we infer that the main faults of the ESFZ are spatially associated with the volcanic segments of the CAVA in El Salvador. Strain localized predominantly at the main volcanic segments of the CAVA during the initial extensional deformation phase. At the intersegment areas (extensional step overs), strong local extension occurs after this first extensional stage. Local extension at intersegment areas can promote magma transport from the source toward the surface through the extensional structures, which explains the presence of monogenetic volcanism [*van Wyk de Vries*, 1993; *Le Corvec et al*., 2013] (Figures 10c and 11c).

6.3. Tectonic Evolution of the ESFZ and the Western Limit of the Chortis Block

Here we present a scenario for the recent tectonic evolution of the ESFZ and compare to adjacent faults systems in Nicaragua and Guatemala. We discuss the kinematics of the fault systems along the CAVA within

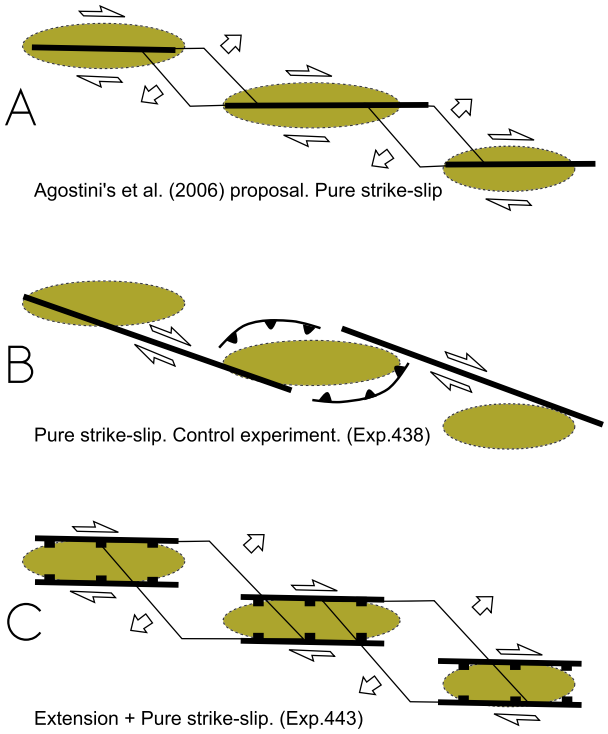

Figure 10. Deformation models: (a) Model proposed by *Agostini et al*. [2006] for ESFZ based on geological data and assuming one phase of pure strike slip. Areas of thinned brittle crust (green areas) control the location of strike-slip deformation. Areas in between strike-slip segments are pull aparts (extension). (b) Single-phase pure strike-slip experiment 435, with discontinuous weak zone combined with pure strike slip. Note that this experiment aims to replicate *Agostini et al.'s* [2006] conceptual model but does not succeed in replicating it. (c) Multiphase experiment 443 with a discontinuous thinned brittle crust undergoing extension followed by pure strike slip. This experiment explains the presence of segmented grabens [*Canora et al*., 2014], the strike-slip reactivation of graben faults, and the presence of pull-apart structures in between thinned crustal areas.

the context of the plate boundary between the Cocos and Caribbean plates as inferred from our experiments and previous studies.

Recent dynamic models and GPS velocity measurements indicate that the strike-slip regime along the CAVA is driven by the relative eastward migration of the Caribbean plate relative to North American Plate [*Álvarez-Gómez et al*., 2008; *Correa-Mora et al*., 2009; *Franco et al*., 2012]. In El Salvador, decoupling of the subduction interface between the Cocos plate and the Chortis Block of the Caribbean [*Lyon-Caen et al*., 2006; *Álvarez-Gómez et al*., 2008] and slab rollback are present and are possibly related to a decrease in the opening rate of the East Pacific Rise during upper Pliocene to Pleistocene as described by *Jarrard* [1986].

The subduction of the Cocos plate beneath the Chortis Block could have conditioned the location, size, and shape of weak zones. Mantle and crustal melt in association with the subducting slab can produce discontinuous emplacement of magma chambers or localized areas of partial melt (weak zones) along the volcanic arc.

It is difficult to reconstruct the temporal evolution of slab rollback of the Cocos plate beneath and along the CAVA, because of the lack of precise age data of volcanic activity. The paleovolcanic arc in El Salvador consists mainly of Miocene lavas of the Balsamo Formation [*Bosse et al*., 1978], with ages of 7.2–6.1 Ma (K-Ar data [*Lexa et al*., 2011]). The oldest volcanic rocks within the active volcanic front are the ones of the Cuscatlan Formation with K-Ar ages of 1.9–0.8 Ma [*Lexa et al*., 2011]. Hence, the rollback process could have taken place in Miocene to Pliocene times, which is between ~7.2–6.1 Ma and 1.9–0.8 Ma.

From the results of our experiments, we broadly distinguished two faulting styles that can be correlated with structures found in the Nicaraguan Depression and the ESFZ. The multiphase experiments 444 and 447 with continuous crustal thinning produce an almost continuous graben with inner strike-slip faults. The inner strike-slip faults are generated during the second phase of strike slip or transtensional deformation and could be an analog for the structures found in the Nicaraguan Depression. Multiphase experiments with a discontinuous weak zone (in particular experiment 443) reproduce better the diffuse and complex deformation of the ESFZ.

Along the CAVA we distinguish three faulting styles from Guatemala, via El Salvador to Nicaragua in association with a decreasing influence of the rollback process from west to east. On the western part of Nicaragua, the current deformation is inside a well-developed semigraben filled with sediments and Quaternary ignimbrites that bury large number of the structures [*van Wyk de Vries*, 1993] (the Nicaraguan Depression). In El Salvador, the faults are not restricted to one main graben but deformation is distributed over a wide fault zone. In El Salvador, areas of discrete deformation (well-developed fault segments) alternate with areas of diffuse deformation (intersegment zones). In Guatemala, the deformation along the CAVA is concentrated along a discrete fault zone, the strike-slip Jalpatagua Fault [*Muehlberger and Ritchie*, 1975] where extension is minor.

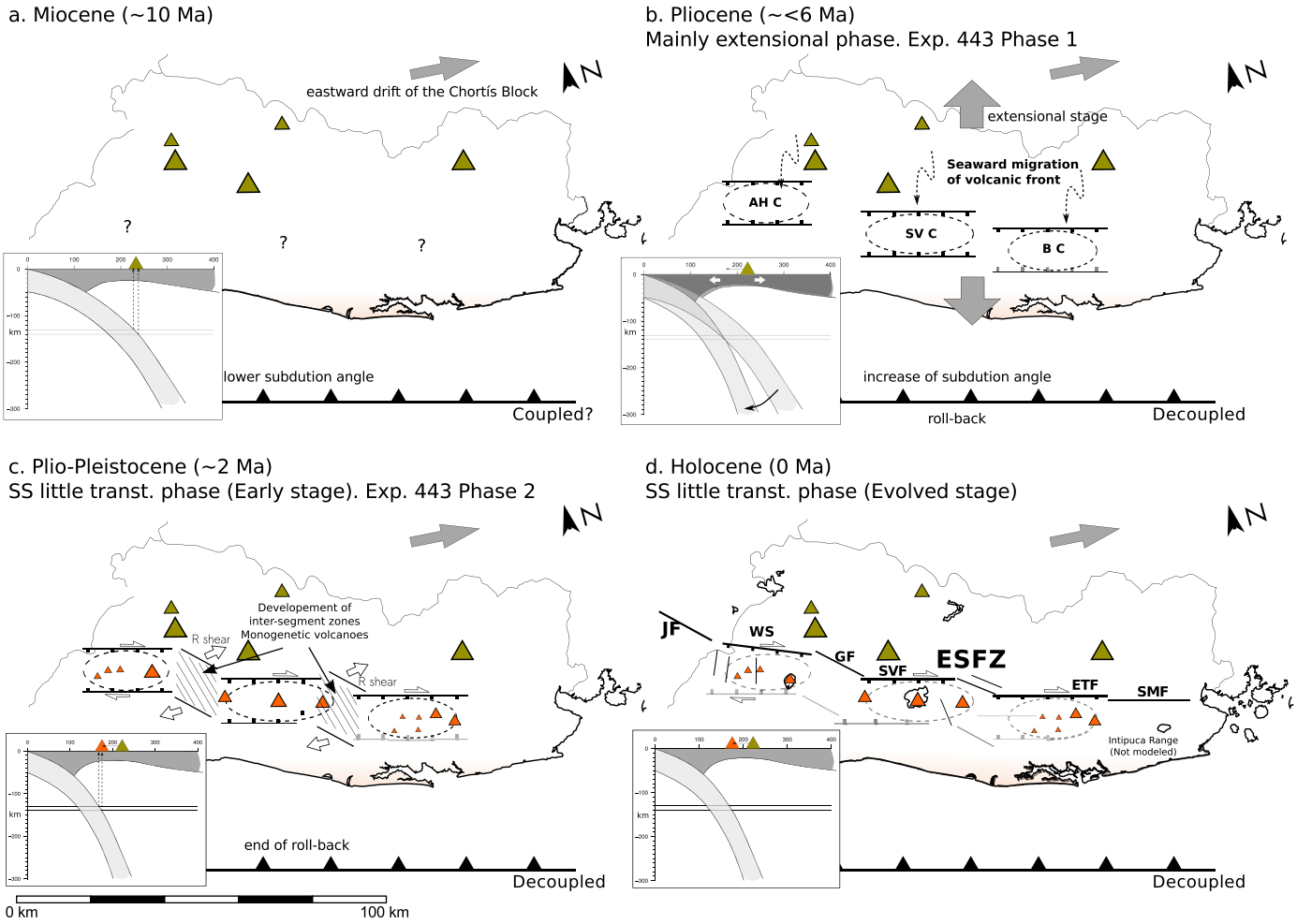

Figure 11. Proposed tectonic evolution of the ESFZ. Green triangles are Miocene volcanoes. (a) Miocene volcanism and low slab dip angle. (b) Extensional phase during Pliocene. Segmented graben structures and emplacement of the main segments of the CAVA in El Salvador. Increase of the slab dip angle. Orange triangles are Plio-Pleistocene volcanoes. (c) Plio-Pleistocene, strike slip, or transtensional (low divergence angle) phase, early stage. Development of intersegment zones and graben faults reactivation. (d) Holocene, evolved stage of the strike slip or transtensional (low divergence angle) phase, current appearance of the ESFZ.

The crustal extension and the seaward migration of the volcanic front would result in thinning and heating of the upper crust. This process seems to have been more pronounced in Nicaragua than in El Salvador, as expressed by the well-developed graben structure in the Nicaraguan Depression compared to the less developed graben structure in El Salvador. The independent magma chambers described by *Agostini et al.* [2006] for El Salvador can be explained by irregular crustal thinning along the volcanic arc. Slab rollback in association with irregular crustal thinning could have produced smaller graben structures in El Salvador as suggested by *Canora et al.* [2014]. For this reason, we think that the independent magma chambers described in *Agostini et al.* [2006] could be related to an irregular crustal thinning along the volcanic arc.

The dip of the Wadati-Benioff Zone increases from Guatemala toward Nicaragua [*Álvarez-Gómez*, 2009; *Funk et al.*, 2009]. This can be associated with to an increase in the subducting slab rollback beneath the Chortis Block from Guatemala to Nicaragua. An increasing slab rollback from northwest to southeast would explain not only the increase in the dip of the Wadatti-Benioff Zone but also the differences in the faulting style along the CAVA, and the trenchward migration of the volcanic arc in El Salvador and Nicaragua.

7. Conclusions

Our experimental approach allows us to clarify some observations made in the ESFZ, such as the presence of extensional structures in the current pure strike-slip regime, the dip angle of the main faults, the

seaward migration of the volcanic arc, and the segmentation of the fault zone. Based on the experiments and the discussion presented above, we conclude that the ESFZ is not a neoformed fault zone, but the result of a two-phase structural evolution similar to that proposed by *Canora et al*. [2014] based on geological observations.

Experiments with a discontinuous weak zone, representing a weaker crust, and a two-phase evolution consisting of an initial extensional phase followed by a strike-slip phase, best explains the present-day structures observed in the ESFZ. In particular, this model explains the presence of dip-slip fault scarps and stepping graben structures that formed during the extensional phase and the subsequent reactivation of those structures as pure strike-slip faults. The location of areas of partial melt within the volcanic arc (represented by the discontinuous weak zone in the experimental models) controls the segmentation of the ESFZ. During the extensional phase, the grabens formed above the areas of thinned (weak) crust. During the subsequent predominantly strike-slip phase, the grabens faults are reactivated and intersegment zones (areas between grabens) are developed.

The initial extensional phase can be correlated to slab rollback of the Cocos plate beneath the Chortis Block. The volcanic ages in El Salvador allow us to infer that the rollback process occurred between 7.2–6.1 Ma and 1.9–0.8 Ma (ages from *Bosse et al*. [1968] and *Lexa et al*. [2011]). Mantle and crustal melt in association with the subducting slab produced discontinuous emplacement of magma chambers, or localized areas of partial melt, along the volcanic arc. These areas of thinned brittle crust control the formation of grabens along the CAVA in El Salvador. Once rollback stopped, the initial extensional structures were reactivated as major strike-slip faults during the second phase (from 1.9–0.8 Ma to the present), a phase characterized by a predominant strike-slip regime. During the second phase, the intersegment zones undergo distributed deformation and local transtension and releasing bends and pull-apart basins formed (Figure 11).

The experiments undertaken with a continuous crustal thinning do not reproduce structures similar to the ESFZ. However, those models present a structural style closer to the structures in the Nicaraguan Depression. The more pronounced development of graben structures in Nicaragua could be a consequence of a more intense extensional phase in Nicaragua than in El Salvador. According to the structures present along the CAVA from Guatemala to Nicaragua and the dip of the Wadati-Benioff Zone, we propose that the rollback beneath the Chortis Block had less influence on the kinematics of Guatemala and an increased influence eastward toward Nicaragua.

Acknowledgments

This research has been supported by the project "INTERGEO" (CGL2013-47412-C2-1-P), Study of the seismic potential of inter-segment regions in strike-slip active faults using Geological, Geophysial and Geodetic analysis: Applied to the Alhama de Murcia Fault and the El Salvador Fault Zone, and New Zealand MBIE Funds-Geothermal Programme. We are grateful to our colleagues at DGOA-MARN (Observatorio Ambiental): Manuel Díaz and Douglas Hernández for their assistance. Some figures were produced using GMT software [*Wessel et al*., 2013]. Thanks to Nicole Schwendener for technical assistance during CT data acquisition. The first author acknowledges financial support for this publication from the Campus of International Excellence of Madrid (UCM–UPM), Spain. The data for this paper are available by contacting the corresponding author. We are grateful to Giacomo Corti and Benjamin van Wyk de Vries for their constructive comments that helped improve this paper.

References

Agostini, S., G. Corti, C. Doglioni, E. Carminati, F. Innocenti, S. Tonarini, P. Manetti, G. Di Vincenzo, and D. Montanari (2006), Tectonic and magmatic evolution of the active volcanic front in El Salvador: Insight into the Berlín and Ahuachapán geothermal areas, *Geothermics*, *35*(4), 368–408.

Alonso-Henar, J., J. A. Álvarez-Gómez, and J. J. Martínez-Díaz (2014), Constraints for the recent tectonics of the El Salvador Fault Zone, Central America Volcanic Arc, from morphotectonic analysis, *Tectonophysics*, *623*, 1–13.

Álvarez-Gómez, J. A. (2009), Tectónica activa y geodinámica en el norte de Centro América, PhD thesis, Dep. Geodyn., Universidad Complutense de Madrid, Madrid.

Álvarez-Gómez, J. A., P. T. Meijer, J. J. Martínez-Díaz, and R. Capote (2008), Constraints from finite element modeling on the active tectonics of northern Central America and the Middle America Trench, *Tectonics*, *27*, TC1008, doi:10.1029/2007TC002162.

Authemayou, C., G. Brocard, C. Teyssier, T. Simon-Labric, A. Guttierrez, E. N. Chiquin, and S. Moran (2011), The Caribbean-North America-Cocos triple junction and the dynamics of the Polochic-Motagua fault systems: Pull-up and zipper models, *Tectonics*, *30*, TC3010, doi:10.1029/2010TC002814.

Bonini, M., T. Souriot, M. Boccaletti, and J. P. Brun (1997), Successive orthogonal and oblique extension episodes in a rift zone: Laboratory experiments with application to the Ethiopian Rift, *Tectonics*, *16*(2), 347–362.

Bosse, H. R., W. Lorenz, A. Merino, A. Mihm, K. Rode, M. Schmidt-Thomé, G. Wiesemann, and H. S. Weber (1978), Geological map of El Salvador Republic: Hannover Germany, Bundesanstalt für Geowissenschaften und Rohstoffe, D-3 scale 1:100,000.

Bryan, C. J., S. Sherburn, H. M. Bibby, S. C. Bannister, and A. W. Hurst (1999), Shallow seismicity of the central Taupo Volcanic Zone, New Zealand: Its distribution and nature, *N. Z. J. Geol. Geophys.*, *42*(4), 533–542, doi:10.1080/00288306.1999.9514859.

Bundschuh, J., and G. E. Alvarado (2007), *Central America. Geology-Resources-Hazards*, vol. 1, 1st ed., p. 663, Taylor and Francis, London, U. K.

Burbidge, D. R., and J. Braun (1998), Analogue models of obliquely convergent continental plate boundaries, *J. Geophys. Res.*, *103*(B7), 15,221–15,237, doi:10.1029/98JB00751.

Burkart, B., and S. Self (1985), Extension and rotation of crustal blocks in Northern Central-America and effect on the volcanic arc, *Geology*, *13*, 22–26.

Byerlee, J. (1978), Friction of rocks, *Pure Appl. Geophys.*, *116*, 615–626.

Canora, C., J. J. Martínez-Díaz, P. Villamor, K. Berryman, J. A. Álvarez-Gómez, C. Pullinger, and R. Capote (2010), Geological and seismological analysis of the Mw 6.6 13th February 2001 El Salvador earthquake: Evidence for surface rupture and implications for seismic hazard, *Bull. Seismol. Soc. Am.*, *100*(6), 2873–2890.

Canora, C., P. Villamor, J. J. Martínez-Díaz, K. Berryman, J. A. Álvarez-Gómez, R. Capote, and W. Hernández (2012), Paleoseismic analysis of the San Vicente segment of the El Salvador Fault Zone, El Salvador, Central America, *Geol. Acta*, *10*, 103–123.

Canora, C., J. J. Martínez-Díaz, P. Villamor, K. Berryman, J. A. Álvarez-Gómez, R. Capote, and M. Díaz (2014), Structural development of El Salvador Fault Zone, *J. Iberian Geol.*, *40*(3), 471–488, in press.
Carr, M. J. (1976), Underthrusting and quaternary faulting in northern Central America, *Geol. Soc. Am. Bull.*, *87*, 825–829.
Correa-Mora, F., C. DeMets, D. Alvarado, H. L. Turner, G. Mattioli, D. Hernández, C. Pullinger, M. Rodríguez, and C. Tenorio (2009), Evidence for weak coupling of the Cocos plate subduction interface and strong coupling of the volcanic arc faults from modeling of GPS data: El Salvador and Nicaragua, *Geophys. J. Int.*, *179*, 1279–1291.
Corti, G., M. Bonini, S. Conticelli, F. Innocenti, P. Manetti, and D. Skoutis (2003), Analogue modelling of continental extension: A review focused on the relations between the patterns of deformation and the presence of magma, *Earth Sci. Rev.*, *63*, 169–247.
Corti, G., E. Carminati, F. Mazzarini, and M. O. Garcia (2005a), Active strike-slip faulting in El Salvador, Central America, *Geology*, *33*, 989–992.
Corti, G., G. Moratti, and F. Sani (2005b), Relations between surface faulting and granite intrusions in analogue models of strike-slip deformation, *J. Struct. Geol.*, *27*, 1547–1562.
DeMets, C., R. G. Gordon, and D. F. Argus (2010), Geologically current plate motions, *Geophys. J. Int.*, *181*, 1–80.
Franco, A., et al. (2012), Fault kinematics in northern Central America and coupling along the subduction interface of the Cocos Plate, from GPS data in Chiapas (Mexico), Guatemala and El Salvador, *Geophys. J. Int.*, *189*, 1223–1236.
Funk, J., P. Mann, K. McIntosh, and J. Stephens (2009), Cenozoic tectonics of the Nicaraguan depression, Nicaragua, and Median Trough, El Salvador, based on seismic reflection profiling and remote-sensing data, *Geol. Soc. Am. Bull.*, *121*(11/12), 1491–1521.
Guzman-Speziale, M., and J. J. Meneses-Rocha (2000), The North America-Caribbean plate boundary west of the Motagua-Polochic fault system: A fault jog in southeastern Mexico, *J. S. Am. Earth Sci.*, *13*, 459–468.
Guzman-Speziale, M., W. D. Pennington, and T. Matumoto (1989), The triple junction of the North America, Cocos, and Caribbean plates: Seismicity and tectonics, *Tectonics*, *8*, 981–997, doi:10.1029/TC008i005p00981.
Hasegawa, A., A. Yamamoto, N. Umino, S. Miura, S. Horiuchi, D. Zhao, and H. Sato (2000), Seismic activity and deformation process of the overriding plate in the northeastern Japan subduction zone, *Tectonophysics*, *319*, 225–239.
Holohan, E. P., B. van Wyk de Vries, and V. R. Troll (2008), Analogue models of caldera collapse in strike-slip tectonic regimes, *Bull. Volcanol.*, *70*, 773–796.
Jarrard, R. D. (1986), Relations among subduction parameters, *Rev. Geophys.*, *24*(2), 217–284, doi:10.1029/RG024i002p00217.
Keep, M., and K. R. McClay (1997), 3D analogue modeling of multiphase rift systems, *Tectonophysics*, *273*, 239–270.
Le Corvec, N., T. Menand, and J. Lindsay (2013), Interaction of ascending magma with pre-existing crustal fractures in monogenetic basaltic volcanism: An experimental approach, *J. Geophys. Res. Solid Earth*, *118*, 1–17, doi:10.1002/jgrb.50142.
Lexa, J., J. Šebesta, C. J. Alexander, W. Hernández, and W. Pécskay (2011), Geology and volcanic evolution in the southern part of the San Salvador Metropolitan Area, *J. Geosci.*, *56*, 105–140.
Lyon-Caen, H., et al. (2006), Kinematics of the North American–Caribbean–Cocos plates in Central America from new GPS measurements across the Polochic–Motagua fault system, *Geophys. Res. Lett.*, *33*, L19309, doi:10.1029/2006GL027694.
Martinez-Diaz, J., J. Alvarez-Gomez, B. Benito, and D. Hernandez (2004), Triggering of destructive earthquakes in El Salvador, *Geology*, *32*(1), 65–68.
Mathieu, L., and B. van Wyk de Vries (2011), The impact of strike-slip, transtensional and transpressional fault zones on volcanoes. Part 1: Scaled experiments, *J. Struct. Geol.*, *33*, 907–917.
Mazzarini, F., G. Musumeci, D. Montanari, and G. Corti (2010), Relations between deformation and upper crustal magma emplacement in laboratory physical models, *Tectonophysics*, *484*, 139–146.
McBirney, A. R., and H. Williams (1965), *Volcanic History of Nicaragua*, vol. 55, 73 pp., Publ. in Geol. Sci., Univ. of Calif, Berkeley, Calif.
Morgan, J. P., C. R. Ranero, and P. Vannucchi (2008), Intra-arc extension in Central America: Links between plate motions, tectonics, volcanism, and geochemistry, *Earth Planet. Sci. Lett.*, *272*, 365–371.
Muehlberger, W. R., and A. W. Ritchie (1975), Caribbean-Americas plate boundary in Guatemala and southern Mexico as seen on Skylab IV orbital photography, *Geology*, *3*, 232–235.
Naylor, M. A., G. Mandl, and C. H. K. Sijpesteijn (1986), Fault geometries in basement-induced wrench faulting under different initial stress states, *J. Struct. Geol.*, *8*, 737–752.
Ortega-Gutiérrez, F., M. Elías-Herrera, and M. G. Dávalos-Elizondo (2008), On the nature and role of the lower crust in the volcanic front of the Trans-Mexican Volcanic Belt and its fore-arc region, southern and central Mexico, *Rev. Mex. Cienc. Geol.*, *25*(2), 346–364.
Panien, M., G. Schreurs, and A. Pfiffner (2006), Mechanical behaviour of granular materials used in analogue modelling: Insights from grain characterisation, ring-shear tests and analogue experiments, *J. Struct. Geol.*, *28*, 1710–1724.
Pfiffner, O. A., and J. G. Ramsay (1982), Constraints on geological strain rates: Arguments from finite strain states of naturally deformed rocks, *J. Geophys. Res.*, *87*(B1), 311–321, doi:10.1029/JB087iB01p00311.
Pindell, J. L., and S. F. Barret (1990), Geological evolution of the Caribbean region: A plate tectonic perspective, in *The Geology of North America, Vol. H, The Caribbean Region*, pp. 339–374, Geol. Soc. of Am., Boulder, Colo.
Plafker, G. (1976), Tectonic aspects of the Guatemala earthquake of 4 February 1976, *Science*, *193*(4259), 1201–1208.
Riedel, W. (1929), Zur Mechanik Geologischer Brucherscheinungen, *Zentral-blatt fur Mineralogie, Geologie und Paleontologie, Abteilung*, *1929B*, 354–368.
Rogers, R. D., H. Karason, and R. D. van der Hilst (2002), Epeirogenic uplift above a detached slab in northern Central America, *Geology*, *30*, 1031–1034.
Rose, W. I., F. M. Conway, C. R. Pullinger, A. Deino, and W. C. McIntosh (1999), An improved age framework for late Quaternary silicic eruptions in northern Central America, *Bull. Volcanol.*, *61*, 106–120.
Scholz, C. H. (2002), *The Mechanics of Earthquake and Faulting*, 2nd ed., p. 447, Cambridge Univ. Press, Cambridge, New York.
Schreurs, G. (2003), Fault development and interaction in distributed strike-slip shear zones: An experimental approach, in *Intraplate Strike-Slip Deformation Belts*, edited by F. Storti, R. E. Holdsworth, and F. Salvini, *Geol. Soc. London Spec. Publ.*, *210*, 35–52.
Schreurs, G., and B. Colletta (1998), Analogue modelling of faulting in zones of continental transpression and transtension, in *Continental Transpressional and Transtensional Tectonics*, edited by R. E. Holdsworth, R. A. Strachan, and J. F. Dewey, *Geol. Soc. London Spec. Publ.*, *210*, 39–79.
Schreurs, G., R. Hänni, M. Panien, and P. Vock (2003), *Analysis of Analogue Models by Helical X-ray Computed Tomography*, *Geol. Soc. London Spec. Publ.*, *215*, 213–223.
Staller, A. (2014), Modelización de las deformaciones corticales en El Salvador (Centroamérica) mediante la integración de datos geodésicos (GPS), geológicos y sismológicos, PhD thesis, Dept. Ingeniería Topográfica y Cartografía. Universidad Politécnica de Madrid, Madrid.
Stoiber, R. E., and M. J. Carr (1973), Quaternary volcanic and tectonic segmentation of Central America, *Bull. Volcanol.*, *37–3*, 304–325.
Tchalenko, J. S. (1970), Similarities between shear zones of different magnitudes, *Geol. Soc. Am. Bull.*, *81*, 1625–1640.
van Wyk de Vries, B. (1993), Tectonics and magma evolution of Nicaraguan volcanic systems, PhD thesis, Open Univ., Milton Keynes, U. K.
van Wyk de Vries, B., and R. Matela (1998), Extension induced by volcanic loading in regional strike-slip zones, *Geology*, *26*(11), 983–986.

Vendeville, B., P. R. Cobbold, P. Davy, P. Choukroune, and J. P. Brun (1987), Physical models of extensional tectonics at various scales, in *Continental Extensional Tectonics*, edited by P. Coward, J. F. Dewey, and P. L. Hancock, *Geol. Soc. London Spec. Publ.*, *28*, 633–643.

Wadge, G., and K. Burke (1983), Neogene Caribbean plate rotation and associated Central American tectonic evolution, *Tectonics*, *2*, 633–643, doi:10.1029/TC002i006p00633.

Weijermars, R. (1986), Flow behaviour and physical chemistry of bouncing putties and related polymers in view of tectonic laboratory applications, *Tectonophysics*, *124*, 325–358.

Weinberg, R. E. (1992), Neotectonic development of western Nicaragua, *Tectonics*, *11*(5), 1010–1017, doi:10.1029/92TC00859.

Wessel, P., W. H. F. Smith, R. Scharroo, J. F. Luis, and F. Wobbe (2013), Generic mapping tools: Improved version released, *Eos Trans. AGU*, *94*, 409–410, doi:10.1002/2013EO450001.

Wu, J., K. McClay, P. Whitehouse, and T. Dooley (2009), 4D analogue modelling of transtensional pull-apart basins, *Mar. Pet. Geol.*, *26*(8), 1608–1623.